PNAS RESEARCH ARTICLE | CHEMISTRY MEDICAL SCIENCES

Restoring neuronal iron homeostasis revitalizes neurogenesis after spinal cord injury

Huimin Geng[a,b,1], Zhiwei Li[b,c,1], Zheng Li[b,c], Yuqi Zhang[b], Zhiliang Gao[a], Lei Sun[d], Xingang Li[b], Jiwei Cui[a,2], Shilei Ni[b,c,2], and Jingcheng Hao[a,2]

Edited by C. Jeffrey Brinker, The University of New Mexico, Albuquerque, NM; received November 29, 2022; accepted October 6, 2023

Spinal cord injury (SCI) can lead to iron overloading and subsequent neuronal ferroptosis, which hinders the recovery of locomotor function. However, it is still unclear whether the maintenance of neuronal iron homeostasis enables to revitalize intrinsic neurogenesis. Herein, we report the regulation of cellular iron homeostasis after SCI via the chelation of excess iron ions and modulation of the iron transportation pathway using polyphenol-based hydrogels for the revitalization of intrinsic neurogenesis. The reversed iron overloading can promote neural stem/progenitor cell differentiation into neurons and elicit the regenerative potential of newborn neurons, which is accompanied by improved axon reinnervation and remyelination. Notably, polyphenol-based hydrogels significantly increase the neurological motor scores from ~8 to 18 (out of 21) and restore the transmission of sensory and motor electrophysiological signals after SCI. Maintenance of iron homeostasis at the site of SCI using polyphenol-based hydrogels provides a promising paradigm to revitalize neurogenesis for the treatment of iron accumulation-related nervous system diseases.

hydrogel | polyphenol | spinal cord injury | neurogenesis | iron overloading

Significance

The regeneration of neurons and axons is severely limited following spinal cord injury (SCI) that can induce impairment of neurological function. Here, we demonstrate that the iron overloading after SCI plays a vital role in the axon disruption and neuronal regeneration failure. To address this issue, we develop a locoregional implant of polyphenol-based hydrogels that can restore the neuronal iron homeostasis to revitalize intrinsic neurogenesis and improve locomotor behaviors after SCI. The work reveals the importance of iron homeostasis in restorative neuroscience by using polyphenol-based hydrogels, which provides a promising strategy to facilitate neurogenesis for the treatment of nervous injury-related diseases.

Spinal cord injury (SCI) is a severe central nervous system issue that often leads to irreversible dysregulation in motor and sensory functions and is associated with high rates of mortality and disability (1, 2). Regeneration of neurons and axons after SCI is typically inhibited due to inflammatory cascades and oxidative stress (2–5). Recent studies have shown that ferroptosis, an iron-dependent cell death pathway, exists in the pathological conditions of SCI and induces the deterioration of locomotor function (6, 7). Genetically, ferroptosis is mainly related to the genomic change of iron homeostasis and lipid peroxidation metabolism, which can be inhibited by preventing the iron-catalyzed Fenton reaction using iron chelators (e.g., deferoxamine) and/or reducing lipid peroxidation using antioxidants (e.g., ferrostatin-1, liproxstatin-1) (8–10). However, the systemic administration of iron chelators for the SCI treatment suffers from a relatively short half-life time of circulation and a low utilization rate. Although the presence of ferroptosis in the impairment of motor function after SCI has been revealed, the detailed implication of iron overloading in subsequent axon disruption and neuronal regeneration failure has not yet been elucidated (11). Additionally, iron overloading is associated with neurodegenerative diseases, such as Parkinson's and Alzheimer's diseases. Therefore, it is of significance to address the issue of iron in regenerating neurons.

Phenolic compounds containing catechol and/or gallol groups are widely distributed in organisms and are generally involved in various biological functions (12–14). One of the most profound features of polyphenols is their potent antioxidant properties, which can help prevent various oxidative stress-associated diseases, such as cancer and Alzheimer's disease (15). Furthermore, polyphenols (e.g., tannic acid, TA) can coordinate with metal ions (e.g., Fe^{3+}, Fe^{2+}) to form metal–phenolic networks, which have been used for the engineering of films and particles (16, 17). Additionally, when the Fe^{2+} is complexed with polyphenols, it is hard to participate in Fenton reactions for the production of harmful hydroxyl radicals (18–20), which could be due to the fast oxidization of Fe^{2+} into Fe^{3+} in the polyphenol complexes (19, 21). Since phenolic compounds can chelate iron ions and scavenge reactive oxygen species (ROS), it is hypothesized that they can simultaneously inhibit iron accumulation and lipid peroxidation to prevent SCI-induced ferroptosis.

Herein, we demonstrate that iron overloading in the spinal cord is not only indicative of impaired motor function but also crucially contributes to axonal disruption and failure of neuronal regeneration. Polyphenol-based hydrogels can restore neuronal iron homeostasis to improve the differentiation and proliferation of progenitor cells and neurite outgrowth. Composed of TA, arginine-doped polydopamine (PDAR) nanoparticles (NPs), and carboxymethyl chitosan (CC), polyphenol-based (TPC) hydrogels were used to ameliorate the pathological iron overloading of SCI (Fig. 1*A*). TPC hydrogels significantly revitalized the intrinsic neuro-regenerative potential by suppressing the degeneration of injured neurons and their axons and by regulating the fate of neural stem/progenitor cells (NSPCs). Notably, hydrogel-mediated iron homeostasis resulted in newborn neurons,

Author contributions: H.G., X.L., S.N., J.C., and J.H. designed research; H.G., Zhiwei Li, Zheng Li, Y.Z., and Z.G. performed research; J.C. and S.N. contributed new reagents/analytic tools; H.G., Zhiwei Li, Zheng Li, L.S., X.L., S.N., J.C., and J.H. analyzed data; and H.G., Zhiwei Li, J.C., S.N., and J.H. wrote the paper.

The authors declare no competing interest.

This article is a PNAS Direct Submission.

[1]H.G. and Zhiwei Li contributed equally to this work.

[2]To whom correspondence may be addressed. Email: nishilei@sdu.edu.cn, jwcui@sdu.edu.cn, or jhao@sdu.edu.cn.

This article contains supporting information online at https://www.pnas.org/lookup/suppl/doi:10.1073/pnas.2220300120/-/DCSupplemental.

Published November 10, 2023.

which could contribute to the reconstruction of functional neural networks and the transmission of electrophysiological signals for improving coordination motor recovery in SCI rats. This research demonstrates that locoregional implantation of an iron-chelating system to maintain iron homeostasis and the redox balance is a promising strategy for SCI treatment.

Results and Discussion

Detriment of Iron Deposition to Neural Regeneration In Vitro. TPC Hydrogels were prepared by integration of TA and PDAR NPs with CC, while TA/CC (defined as TC) hydrogels were composed of TA and CC based on noncovalent interactions (*SI Appendix*, Figs. S1–S4). Resonance Raman spectra demonstrated that the hydrogels could sequester Fe^{3+} from the $FeCl_3$ solution (*SI Appendix*, Fig. S5). TC and TPC hydrogels both showed negligible cytotoxicity and biodegradable in vivo (*SI Appendix*, Figs. S6 and S7). The regulation of intracellular iron levels and neural regeneration using polyphenol-based hydrogels was investigated in vitro. A ferroptosis model of PC12 cells was established using RSL3 (an inhibitor of glutathione peroxidase 4, GPX4), which could cause ROS accumulation and lipid peroxidation (22, 23). After the incubation of PC12 cells with RSL3, the intracellular concentrations of Fe, H_2O_2,

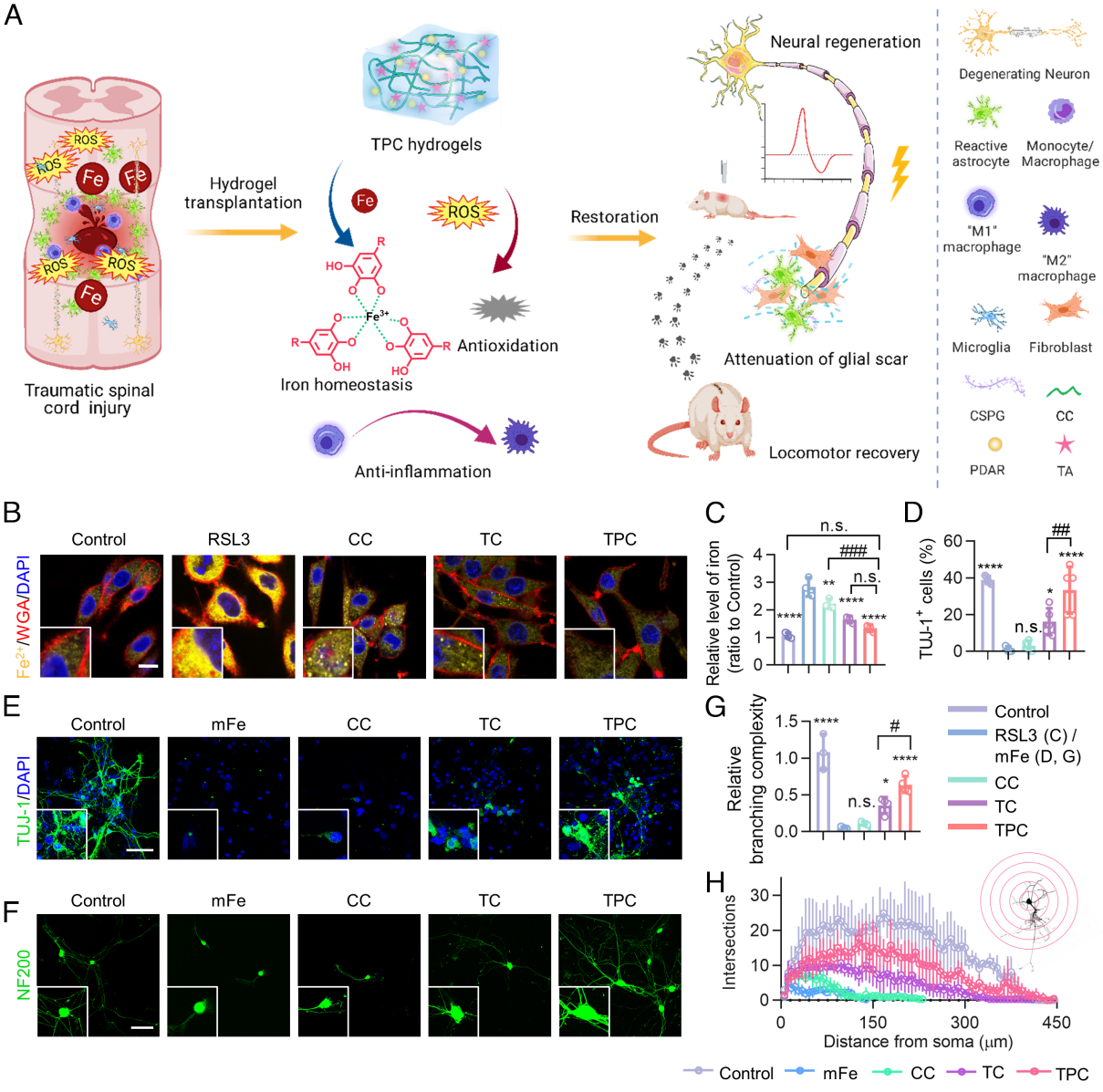

Fig. 1. Polyphenol-based hydrogels for the treatment of SCI. (*A*) Schematic illustration of TPC hydrogels for SCI repair. The hydrogels implanted on the SCI sites can chelate overloaded iron ions, scavenge ROS, and suppress inflammation, resulting in neural regeneration, attenuation of glial scar, and locomotor recovery in rats. (*B*) Representative fluorescence images of RSL3-treated PC12 cells incubated with different materials. Fe^{2+}, membranes, and nuclei were strained with FerroOrange (yellow), Alexa Fluor 633-wheat germ agglutinin (WGA-AF633, red), and DAPI (blue), respectively. (Scale bar: 10 μm.) (*C*) Quantification of Fe in PC12 cells, which were normalized against the control (PBS) group (n = 4). (*D*) Quantification of the percentages of $TUJ\text{-}1^+$ cells derived from NSPCs (n = 5). (*E*) Representative fluorescence images of NSPC-derived cells treated with Fe^{2+} and CC, TC, or TPC at day 7, and stained with anti-TUJ-1 antibodies (green) and DAPI (blue), respectively. (Scale bar: 50 μm.) (*F*) Representative fluorescence images of cultured DRG neurons, stained with anti-NF200 antibodies (green). (Scale bar: 50 μm.) (*G* and *H*) Branching complexity (*G*) and Sholl analysis (*H*) of neurite outgrowth in DRGs incubated with different materials, which were normalized against the control group (n = 3). All data represent the mean ± SD. (*C*, *D*, and *G*) One-way ANOVA followed by Tukey's post hoc test. **P* < 0.05, ***P* < 0.01, ****P* < 0.001, and *****P* < 0.0001 compared with the RSL3 or mFe^{2+} groups. #*P* < 0.05, ##*P* < 0.01 and ###*P* < 0.001 compared with the TPC group. n.s. = not significant.

and malondialdehyde (MDA, a lipid peroxidation marker) significantly increased (Fig. 1*B* and *SI Appendix*, Fig. S8). However, the accumulation of Fe was alleviated when PC12 cells were treated with CC, TC, or TPC hydrogels due to the metal-chelation of the carboxy groups in CC and the phenolic groups in the TC and TPC hydrogels (Fig. 1*C*). Notably, only the TC and TPC hydrogels could rescue the cells from the RSL3-induced ferroptosis, which could be due to protection from free-radical damage via the internalization of disassembled hydrogels (*SI Appendix*, Fig. S9). The antioxidant effects of the polyphenol-based hydrogels were further demonstrated by exposing PC12 cells to external oxidative stress induced by H_2O_2 and Rosup (*SI Appendix*, Figs. S10 and S11).

Further, the effect of iron deposition on neurogenesis at the cellular level, including differentiation of NSPCs and axonal regrowth, was investigated by adding additional moderate Fe^{2+} (mFe, 0.4 μmol) and excess Fe^{2+} (eFe, 4 μmol) to simulate systemic iron overloading. The cells expressed with β3-tubulin (TUJ-1, neuronal marker) in the mFe group were hardly detectable (1.5 ± 1.1%) compared to control (39.0 ± 2.0%), TC (16.2 ± 7.3%), and TPC (33.4 ± 12.7%) groups (Fig. 1 *D* and *E*). This indicated that the mFe significantly impeded NSPC differentiation towards the neuronal lineage, which could be reversed by the polyphenol-based hydrogels. Subsequently, dissociated dorsal root ganglion (DRG) neurons of neonatal rats were used to determine the impact of iron overloading on neurite outgrowth (Fig. 1*F*) (24, 25). Sholl analysis demonstrated that mFe significantly reduced the length of neurites and the number of the neuritic branches of DRG neurons (Fig. 1 *G* and *H*). Importantly, over 10-fold and twofold increase in DRG branching complexity was observed after TPC treatment compared to the mFe and TC groups, respectively. Moreover, the mRNA levels of neuronal markers (i.e., *Neurod1* and *Tuj-1*) dramatically increased and astrocyte marker (i.e., *Gfap*) decreased in the TPC and TC groups (*SI Appendix*, Fig. S12). In addition, when the metal ions surpassed the chelation ability of TPC hydrogels, no effective $TUJ\text{-}1^+$ cells and available axonal regrowth of DRG neurons were observed in the eFe, eFe/CC, eFe/TC, and eFe/TPC groups (*SI Appendix*, Fig. S13). Moreover, a remarkable iron accumulation was detected in all the groups. The inhibitory neurogenesis induced by the excess ferrous ions cannot be rescued by hydrogels. Overall, the TPC hydrogels can ameliorate the inhibitory microenvironment induced by iron ions within the coordination ability and thus promote NSPC differentiation into neurons instead of astrocytes, while significantly enhancing the axon regeneration of DRG neurons.

Maintenance of Iron Homeostasis for Promotion of Neurogenesis In Vivo. The surgical procedure and experimental timeline for endogenous neurogenesis in the injured spinal cords are shown in Fig. 2*A* and *SI Appendix*, Fig. S14, respectively. Magnetic resonance imaging (MRI) showed acute intraspinal hemorrhage and cord edema at 3 days postinjury (dpi), which were readily relieved in the TPC group (*SI Appendix*, Figs. S15 and S16). Massive hemorrhages are usually associated with iron overloading, which leads to ferroptosis after SCI (22, 26). A significant iron accumulation at lesion sites was observed from both the qualitative and quantitative analysis at 3 dpi (Fig. 2 *B* and *C*). More importantly, the iron concentrations were reduced to the normal level after TPC treatment (*SI Appendix*, Fig. S17). It is attributed to that polyphenol-based hydrogels can penetrate into the injured spinal cords to regulate the microenvironments of SCI (*SI Appendix*, Fig. S18). The expression of growth-associated protein 43 $(GAP43)^+$, a marker of neural growth and newborn fibers, was significantly increased at 7 dpi when TC and TPC hydrogels were utilized. Significantly, TPC was more potent than TC in supporting axonal outgrowth in the injured spinal cords (Fig. 2 *D* and *E*). The expression of doublecortin (DCX), a reliable marker for adult neurogenesis, was examined to demonstrate the regenerative response of injured spinal cords, and Ki67, a cell proliferation marker, was performed to assess the proliferative activity of neurons and stem cells within the lesions (Fig. 2 *F*–*M*) (27, 28). In the SCI group, most DCX^+ neuroblasts surrounded the lesion border and failed to differentiate into neurons. Conversely, the TPC hydrogels promoted the developmental progression of DCX^+ cells into neurons, leading to higher $DCX^+/TUJ\text{-}1^+$ immunofluorescence intensity at the lesion epicenter compared with the SCI group (Fig. 2*H*). A dramatic increase in the number of DCX^+ and $Ki67^+$ cells was observed after the TC and TPC hydrogel treatment, indicating that these newborn neuroblasts were in a cycling state at 7 dpi (Fig. 2 *F*, *I*, and *J*). We further analyzed whether such improvements were related to regulation at the level of stem cell pools, where Ki67 and SOX2 were used to identify type-1 stem cells ($Ki67^-$ $SOX2^+$) and type-2 amplifying progenitor cells ($Ki67^+$ $SOX2^+$) (28). The percentages of both type-1 (~threefold) and type-2 stem cells (~eightfold) in the TPC group were significantly higher than those in the CC and SCI groups (Fig. 2 *G*, *K*–*M*), which suggests that the TPC hydrogels not only support endogenous NSPC recruitment and retention but also promote their conversion from quiescent type-1 to amplifying type-2 stem cells. Taken together, these results indicate that excess iron, simulated in vitro by RSL3 and Fe^{2+} additives, and in vivo by SCI, is an important cause of neural regenerative failure. Importantly, the polyphenol-based hydrogels can maintain iron homeostasis and thus regulate endogenous NSPC fate to enhance intrinsic neurogenesis after SCI.

To evaluate whether TPC hydrogels are able to restore neurogenesis in the presence of excess Fe^{2+} (eFe, 4 μmol, exceeded the in vitro maximum absorption of Fe in TPC hydrogels (3.8 μmol of Fe^{2+} in 20 μL hydrogel) based on inductively coupled plasma mass spectrometry, ICP-MS, *SI Appendix*, Fig. S19), an iron-overloaded SCI model was established by injection of eFe. The iron deposition occurred after SCI and Fe^{2+} injection, while TPC hydrogels were competent to maintain neuronal iron homeostasis after SCI but unable to chelate the additional iron ions in eFe/TPC groups. Additionally, excess iron ions contributed to macrophage recruitment and enhanced inflammation after SCI, which were not rescued by TPC hydrogels (*SI Appendix*, Figs. S20–S22). Further, to exclude the impact of SCI, normal spinal cords were injected with saline, moderate Fe^{2+} (mFe, 0.4 μmol), and eFe, respectively, followed by TPC hydrogel treatments. Normal spinal cord tissues were damaged severely by excess iron ions, resulting in a large number of activated glial fibrillary acidic protein $(GFAP)^+$ astrocytes and chondroitin sulfate proteoglycan (CSPG) signals of glial scars in the eFe and eFe/TPC groups. In addition, the lesion area of the eFe group (36.4 ± 3.2%) was significantly larger than that of the mFe group (27.6 ± 3.8%), indicating that excess ferrous ions were more disruptive to normal spinal cords. TPC hydrogels were able to restore the damage induced by mFe instead of eFe (*SI Appendix*, Figs. S23 and S24). These findings suggest that iron accumulation promotes the destruction of spinal cords and TPC hydrogels protect spinal cords against iron dyshomeostasis via chelating iron ions. When the iron ions surpassed the chelation ability of TPC hydrogels, iron homeostasis is destroyed, therefore resulting in tissue inflammation and neuronal impairment.

Iron Regulation Mechanism of Hydrogels after SCI. To explore the underlying mechanism of neural regeneration after SCI, which was promoted by polyphenol-based hydrogels, the expression of

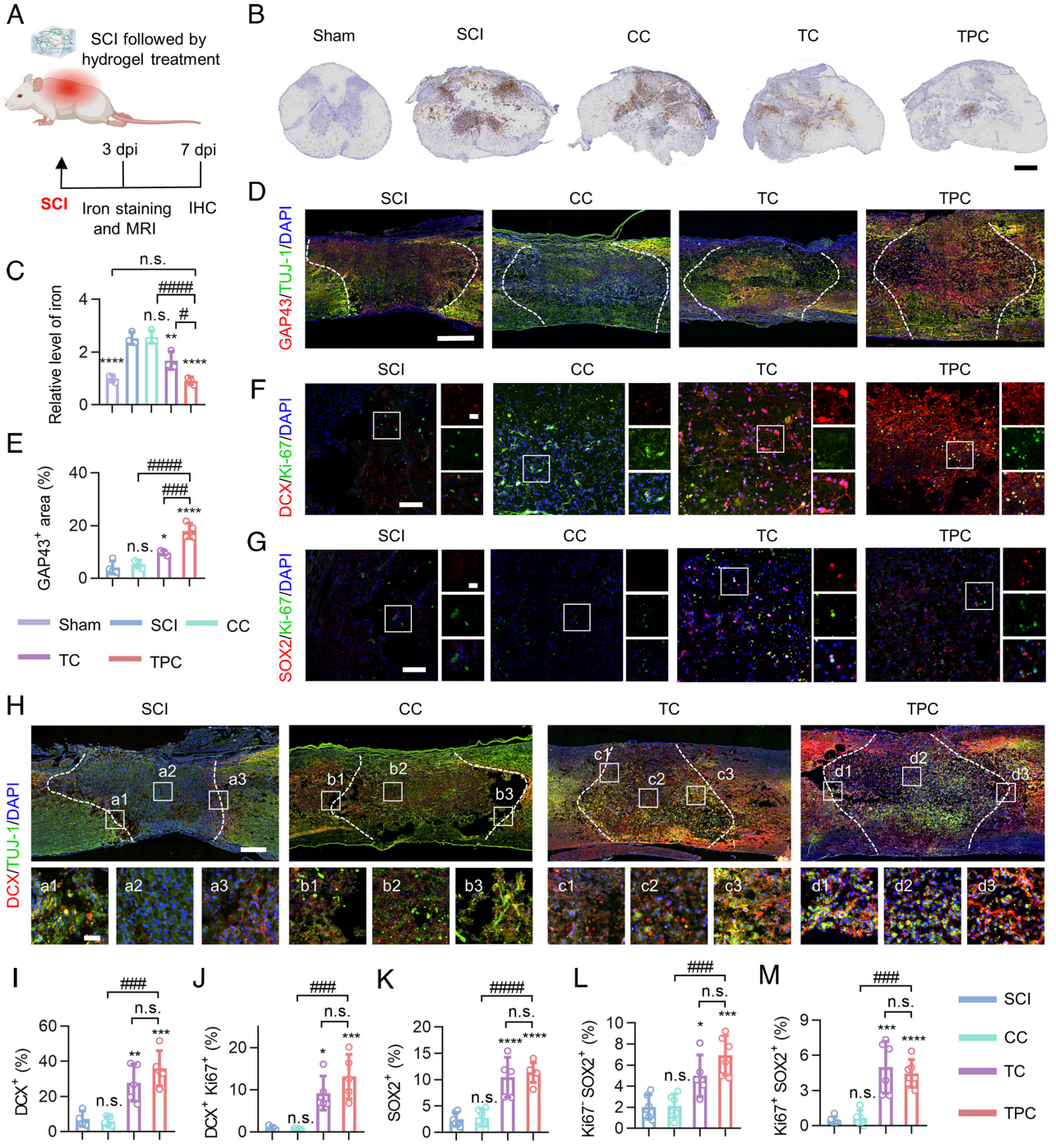

Fig. 2. Iron overload mitigation and neurogenic reprogramming in vivo. (*A*) Experimental design of iron detection after SCI. IHC, immunohistochemistry. (*B*) Representative images of the transverse sections of spinal cord lesions at 7 dpi. Iron ions (brown) were stained with diaminobenzidine-enhanced Prussian blue. (Scale bar: 400 μm.) (*C*) Quantification of iron levels in injured spinal cords measured by an iron colorimetric assay kit, which were normalized against the sham group (n = 3). (*D*) Representative immunofluorescence staining images of the longitudinal spinal cord sections co-labeled with anti-GAP43 (red) and anti-TUJ-1 (green) antibodies. Cell nuclei were stained with DAPI (blue). White dashed lines indicate the border of lesion areas. (Scale bar: 500 μm.) (*E*) Quantification of the percentage of GAP43$^+$ areas in the focal areas. (*F–H*) Representative immunofluorescence staining images of lesion areas in different groups at 7 dpi, stained with antibodies against DCX (red)/Ki67 (green) (*F*), SOX2 (red)/Ki67 (green) (*G*), DCX (red)/TUJ-1 (green) (*H*), respectively. Cell nuclei were stained with DAPI (blue). Enlarged images of the box regions are shown in the right (*F* and *G*) or bottom (*H*) panels. (Scale bars: 500 μm and 50 μm [enlarged images].) (*I–M*) Quantification of the percentage of DCX$^+$ (*I*), DCX$^+$ Ki67$^+$ (*J*), SOX2$^+$ (*K*), Ki67$^-$ SOX2$^+$ (*L*), and Ki67$^+$ SOX2$^+$ (*M*) cells in the focal areas. All data represent the mean ± SD. One-way ANOVA followed by Tukey's post hoc test. **P* < 0.05, ***P* < 0.01, ****P* < 0.001, and *****P* < 0.0001 compared with the SCI groups. #*P* < 0.05, ###*P* < 0.001, and ####*P* < 0.0001 compared with the TPC group. n.s. = not significant.

iron metabolism–related molecules was investigated. At 3 dpi, ROS and MDA were significantly increased in the injured spinal cords, both of which could be alleviated after polyphenol-based hydrogel treatment (Fig. 3 *A* and *B*). Glutathione (GSH), a major intracellular antioxidant, was reduced by SCI and restored to the sham level after TPC treatment (Fig. 3*C*), which suggested that polyphenol-based hydrogels can effectively reduce GSH depletion and scavenge lipid ROS. Moreover, the expression of *Gpx4* mRNA was down-regulated after SCI and regulated by TPC hydrogels. The dysregulation of iron-responsive elements-binding protein 2 (*Ireb2*), divalent metal transporter 1 (*Dmt1*), and transferrin receptor 1 (*TfR1*) implicated that SCI significantly

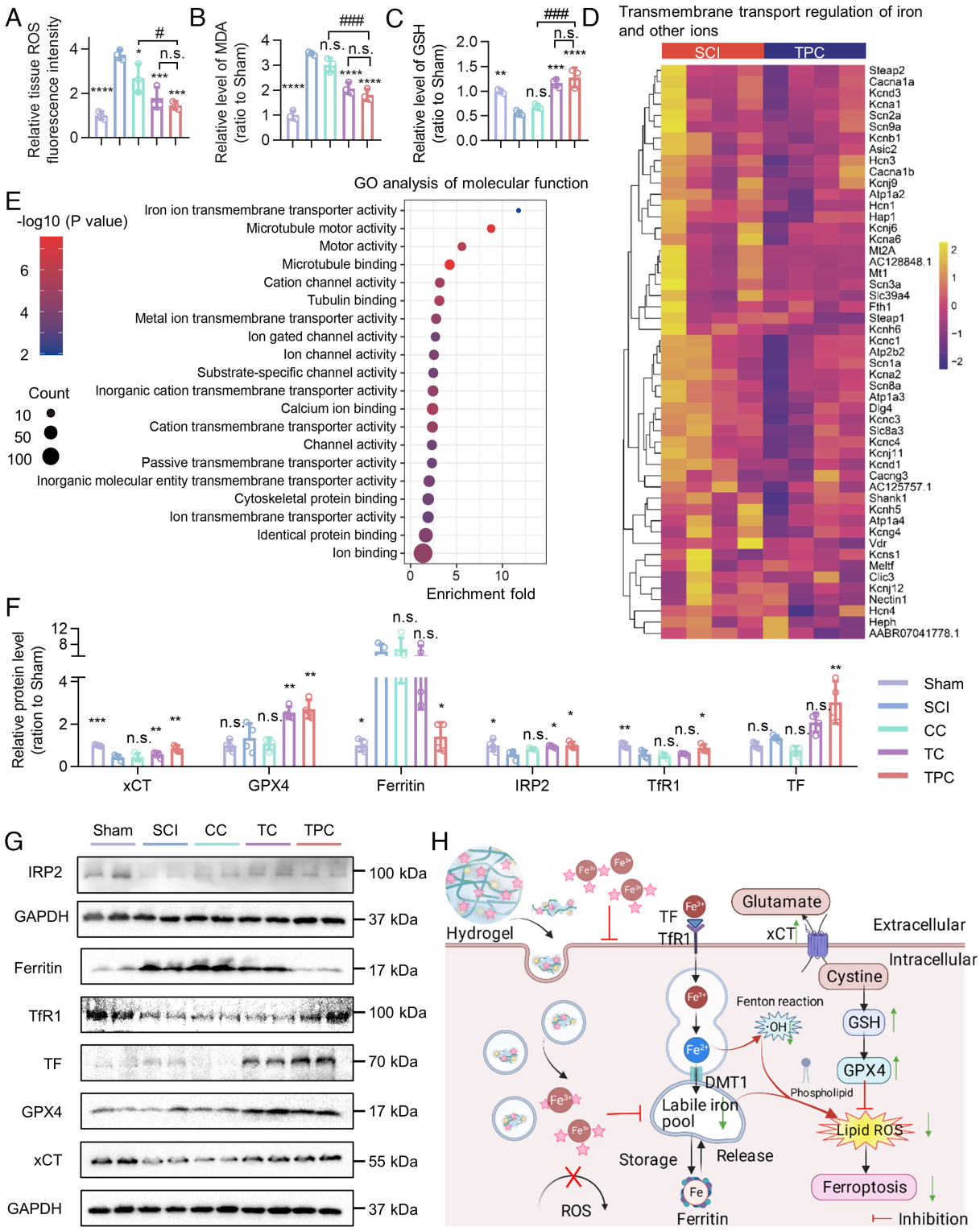

Fig. 3. Potential mechanism of TPC-regulated cellular iron metabolism. (*A–C*) Relative levels of ROS (*A*), MDA (*B*), and GSH (*C*) of injured spinal cords in the sham, SCI, CC, TC, and TPC groups at 3 dpi, which were normalized against the sham group (n = 3). (*D*) Heatmap of differentially expressed genes between SCI and TPC groups. The color bar represents the fold change. (*E*) GO enrichment analysis of molecular function between the differentially expressed genes of SCI and TPC groups at 7 dpi (n = 4). (*F*) The relative protein level of xCT, GPX4, Ferritin, IRP2, TfR1, and TF at 3 dpi, which were normalized against the sham group (n = 4). (*G*) Western blotting images of the different treatment groups. (*H*) Scheme of the TPC-regulated iron metabolism after SCI. All data represent the mean ± SD. One-way ANOVA followed by Tukey's post hoc test (*A–C*, and *F*). **P* < 0.05, ***P* < 0.01, ****P* < 0.001, and *****P* < 0.0001 compared with the SCI group. #*P* < 0.05, ##*P* < 0.01, and ###*P* < 0.001 compared with the TPC group. n.s. = not significant.

impaired the iron homeostasis but could be readily improved by TPC hydrogels. Especially, ferroptosis suppressor protein 1 (*Fsp1*), a glutathione-independent ferroptosis suppressor, was also up-regulated by TPC hydrogels (*SI Appendix*, Fig. S25). mRNA sequencing to analyze differentially expressed genes (DEGs) of the injured spinal cord at 7 dpi between SCI and TPC groups demonstrated that 312 genes were up-regulated and 527 genes were down-regulated after TPC treatment (*SI Appendix*, Fig. S26).

Gene Ontology (GO) and Kyoto Encyclopedia of Genes and Genomes (KEGG) analysis were used to thoroughly investigate the signaling pathways modulated by the TPC hydrogels. As a result, the up-regulated genes associated with the transmembrane transporter activity of metal ions, especially iron ions, in the SCI group were down-regulated in the TPC groups, which indicated that TPC hydrogels affected iron ion absorption (Fig. 3*D*). GO enrichment analysis revealed that TPC hydrogels maintained local iron homeostasis not only by the chelation ability of polyphenols to iron ions, but also by the regulation regional metabolism of metal ions (Fig. 3*E* and *SI Appendix*, Fig. S27). Additionally, TPC treatment could also suppress lipid peroxiadation, facilitate microtubule motor, remodel the extracellular matrix, promote cell proliferation, and increase the resistance to iron ions (*SI Appendix*, Fig. S28). Together, the SCI-induced iron ion over-transportation and its subsequent pathological processes were generally prevented by TPC hydrogels on the mRNA level.

The expression of proteins involved in regulating iron levels was then evaluated at 3 dpi (Fig. 3 *F* and *G* and *SI Appendix*, Fig. S29), where it was found that the expression of xCT and GPX4 in the TPC group was higher than that in the SCI group. This suggested that TPC hydrogels inhibited the typical ferroptosis pathway of the xCT–GSH–GPX4 axis to reduce peroxide lipids after SCI. Moreover, SCI resulted in a significant increase in the expression of the iron storage protein ferritin, which is a surrogate marker for intracellular iron concentrations (29). The TPC hydrogels restored ferritin expression to normal levels, which could be due to the extracellular binding of iron ions and inhibition of its intracellular importation. The internalized phenolic complexes could also coordinate with iron ions, which could curtail the labile iron state of cells (29–31). Thus, TPC treatment induced an elevated level of iron regulatory protein 2 (IRP2), which was negatively correlated with the concentration of cellular iron ions (29). Specifically, as a chief iron sensor, high-level IRP2 caused the increase of transferrin receptor 1 (TfR1) and transferrin (TF) expression, protected mRNA of TfR1 from cleavage, and restricted increases in ferritin by inhibiting its translation initiation. Overall, TPC hydrogels reversed iron accumulation and inhibited ferroptosis, which regulated iron transport and metabolism and activated oxidant scavengers. A proposed mechanism of TPC-regulated cellular iron metabolism is demonstrated in Fig. 3*H*.

Neurological Function Recovery Following SCI and Hydrogel Treatment. The neurological function recovery of the SCI rats following implantation of polyphenol-based hydrogels was monitored for 8 wk (Fig. 4*A*) and the Basso–Beattie–Bresnahan (BBB) score was used to evaluate the locomotor recovery of SCI rats (Fig. 4*B*). As expected, the TC and TPC groups presented significantly improvement of locomotor function compared to the SCI and CC groups at 1 week postinjury (wpi), which demonstrated that the polyphenol-based hydrogels could promote function recovery at an early stage of SCI (Movies S1 and S2). In addition, a significant difference of the maximum angle in the inclined plane test was observed between the SCI (50.8 ± 1.4°) and TPC (66.0 ± 4.9°) groups at 4 wpi (Fig. 4*C*), which suggests that the TPC hydrogels hold great potential for improving hindlimb grip. Remarkably, the SCI rats treated with the TPC hydrogels showed the best improvement in coordinated locomotor function and regular crawling (18.3 ± 1.6 score), and the TC-treated rats exhibited plantar placement with support but stepped without coordination (15.7 ± 0.9 score), while rats in the SCI (8.3 ± 3.0 score) and CC (11.6 ± 2.3 score) groups still dragged their hindlimbs at 8 wpi (Fig. 4*D* and Movie S3). Quantification of footprints revealed that the treatment with TPC hydrogels dramatically reduced the rotation angle, base of support, and relative position of SCI rats at 8 wpi, and elevated the stride length, indicating the notable recovery of locomotor coordination between the fore- and hindlimbs (Fig. 4 *E–H*). Motor-evoked potential (MEP) and somatosensory-evoked potential (SEP) tests were performed to assess the electrophysiological conductivity and the integrity of neural circuits (Fig. 4 *I–O*). Sluggish recovery of electrical conduction was observed in the SCI group with notably distorted waveforms, declining amplitude, and extended latency of both MEP (Fig. 4 *J–L*) and SEP (Fig. 4 *M–O*). In comparison, the TPC hydrogels significantly enhanced electrophysiological recovery with increased amplitude and dropping latency compared to other groups. These results demonstrate that the TPC hydrogels are superior in improving neurological function after SCI compared to the CC and TC groups.

Reprogramming of the SCI Inflammatory Microenvironments. Dysregulation of neuronal iron homeostasis is usually accompanied by neuroinflammation, which could further aggravate a secondary injury cascade after SCI (32–34). Since the SCI-induced iron accumulation and lipid peroxidation could be reversed by the TPC hydrogels, their effects on inflammatory responses and macrophage polarization were investigated. At 3 dpi, there was a significantly difference in the expression of proinflammatory and antiinflammatory cytokines in the injured spinal cords of SCI and TPC groups. Moreover, the up-regulated cytokines in the SCI group were responsible for inflammatory responses, which were down-regulated after TPC treatment (Fig. 5*A*). Consistently, the high expression of proinflammatory cytokines, including TNF-α, IL-1β, and IL-6 at focal areas after SCI were significantly inhibited in the TPC group, while the expression of IL-10, a typical anti-inflammatory cytokine, was higher in the TPC group than that in the SCI group (Fig. 5 *B–E*).

To investigate the responsive pattern of local immune cell subtypes after TPC treatment, the pro- and anti-inflammatory phenotypes of microglia/macrophages were stained with $CD86^+$ $CD11b^+$ (an M1 marker) and $CD206^+$ $CD11b^+$ (an M2 marker), respectively (35). The TPC hydrogels not only significantly curtailed the proportion of the $CD86^+$ $CD11b^+$ population (Fig. 5*F*) but also boosted the $CD206^+$ $CD11b^+$ population compared to the SCI group (Fig. 5*G* and *SI Appendix*, Fig. S30). The results suggest that microglia and macrophages in the injured spinal cord retained a predominantly proinflammatory M1 phenotype, while the polyphenol-based hydrogels could reduce the number of M1 macrophages and enhance M2 polarization after SCI, which alleviated inflammation and promoted functional recovery after injury. Furthermore, the distribution of microglia/macrophage cells in the injured spinal cords was examined by immunofluorescence staining (Fig. 5 *H–K*). A large amount of $IBA1^+$ $CD11b^+$ microglia/macrophages were distributed at rostral boundaries, epicenter, and caudal boundaries in the SCI and CC groups, while the TC and TPC groups showed significantly alleviated local recruitment of $IBA1^+$ $CD11b^+$ cells (Fig. 5 *H* and *J*). Besides, implantation of the hydrogels, especially for the TPC group, resulted in a larger population of $ARG\text{-}1^+$ (an M2 marker) cells at rostral, epicentral, and caudal lesions compared to the SCI group (Fig. 5 *I* and *K*). Overall, the polyphenol-based hydrogels can reprogram the inflammatory microenvironment arising from SCI by suppressing inflammatory cytokines and modulating the polarization of microglia/macrophages, which is favorable for neural regeneration and neural circuit reconstruction.

Reconstruction of the Neural Network after SCI. To investigate how an iron overloading environment effects NSPC differentiation after SCI, the fate of newborn neural cells with or

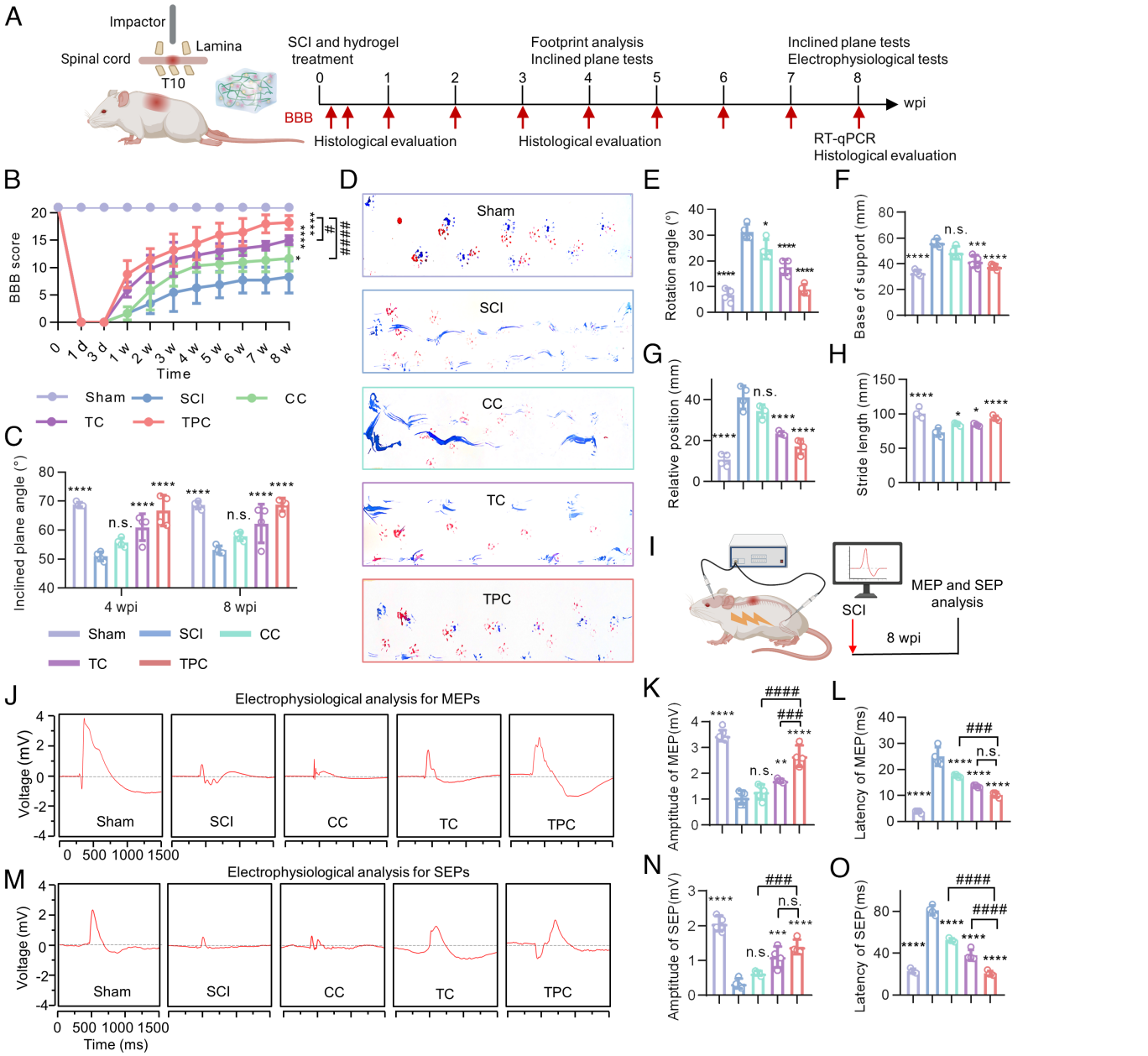

Fig. 4. Improvement of neurological function recovery after SCI. (*A*) Experimental timeline of spinal cord contusion to induce SCI and treatment, behavioral testing, histological evaluation, and electrophysiological tests. (*B*) BBB locomotor scores of the sham, SCI, CC, TC, and TPC groups during treatments for 8 wk in the open field (n = 8). The scores were calculated ranging from 0 (complete paralysis) to 21 (normal locomotion). (*C*) Inclined plane tests in the sham, SCI, CC, TC, and TPC groups at 4 and 8 wpi (n = 4). (*D*) Representative footprints with forelimbs (red) and hindlimbs (blue) at 8 wpi. (*E*–*H*) Quantitative analysis of rotation angle (*E*), base of support (*F*), relative position (*G*), and stride length (*H*) based on footprint patterns (n = 4). (*I*) Experimental design for electrophysiological analysis. (*J*–*O*) MEP (*J*) and SEP (*M*) signals, quantification of the SEP (*K* and *L*) and MEP (*N* and *O*) amplitudes and latency at 8 wpi (n = 4). All data represent the mean ± SD. (*B* and *C*) Two-way ANOVA followed by Tukey's post hoc test. (*E*–*H*, *K*, *L*, *N*, and *O*) One-way ANOVA followed by Tukey's post hoc test. **P* < 0.05, ***P* < 0.01, ****P* < 0.001, and *****P* < 0.0001 compared with the SCI group. ###*P* < 0.001, and ####*P* < 0.0001 compared with the TPC group. n.s. = not significant.

without polyphenol-based hydrogel treatments was determined in vivo. SCI rats were intraperitoneally administered with 5-bromodeoxyuridine (BrdU, a thymidine analogue for the labeling of newly generated cells) until scarified (Fig. 6 *A* and *B*). Immunostaining of the lesion sites showed that about 54.3% of newborn cells ($BrdU^+$) differentiated into neurons ($TUJ\text{-}1^+$) at 4 wpi in the TPC group. Meanwhile, only 27.5% of SCI-induced newborn cells were neurons without axon-like and dendritic structures around cell bodies (Fig. 6*C*). In addition, few $GFAP^+$ $BrdU^+$ astrocytes were observed around the lesion border after TPC hydrogel treatment (Fig. 6*D*). This indicated that TPC hydrogels could significantly promote newborn NSPC differentiation into neurons in vivo, which was highly consistent with the in vitro results.

Next, the contribution of the newborn neurons to neural regeneration and alleviation of scar formation was investigated. A large number of $NeuN^+$ (a marker of mature neurons) cells crossed the scar border and infiltrated into the lesion core in the TPC group, which provided the histological prerequisites to connect the ascending and descending neural circuits (Fig. 6 *E* and *F*). Treatment with TPC hydrogels also significantly decreased $GFAP^+$ astrocytes and $CSPG^+$ in the extracellular matrix, which are the main components of glial scars (Fig. 6*G* and *SI Appendix*, Figs. S31 and S32). Hematoxylin-eosin (H&E) staining also revealed that

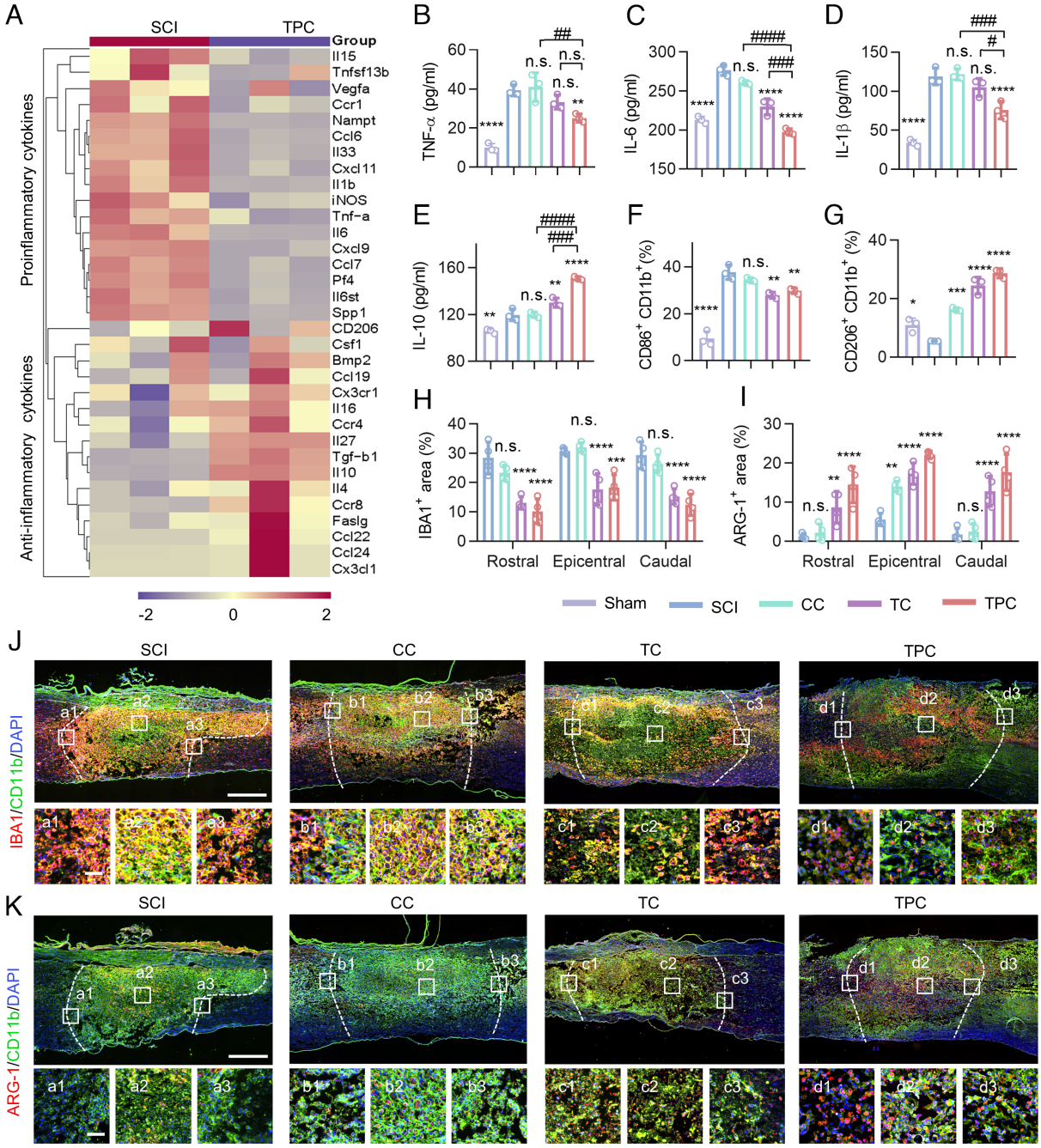

Fig. 5. Regulation of SCI inflammatory responses. (*A*) Heatmap obtained from qRT-PCR assays showing mRNA levels of inflammatory and antiinflammatory cytokines in SCI and TPC groups at 3 dpi (n = 3). (*B–E*) Enzyme-linked immunosorbent assay (ELISA) results of TNF-α (*B*), IL-6 (*C*), IL-1β (*D*), and IL-10 (*E*) of spinal cord specimens at 3 dpi (n = 3). (*F* and *G*) Proportion of $CD206^+$ $CD11b^+$ (*F*) and $CD86^+$ $CD11b^+$ (*G*) cells in injured spinal cords quantified by flow cytometry at 7 dpi (n = 3). (*H* and *I*) Quantification of $IBA1^+$ (*H*), ARG-1^+ (*I*) area percentages (n = 4) according to the immunofluorescence images in (*J*) and (*K*). (*J* and *K*) Representative images of lesion areas in different groups at 7 dpi, which were stained with anti-IBA1 (red)/anti-CD11b (green) antibodies (*J*) and anti-ARG-1 (red)/anti-CD11b (green) antibodies (*K*), respectively. Cell nuclei were stained with DAPI (blue). Enlarged images of the box regions are shown in the bottom panel. (Scale bars: 500 μm [*Top*] and 100 μm [*Bottom*].) All data are mean ± SD (*B–I*) One-way ANOVA followed by Tukey's post hoc test. **P* < 0.05, ***P* < 0.01, ****P* < 0.001, and *****P* < 0.0001 compared with the SCI group. #*P* < 0.05, ###*P* < 0.001, and ####*P* < 0.0001 compared with the TPC group. n.s. = not significant.

the cavity area in the TPC group was the smallest compared to that of the other groups (Fig. 6*H* and *SI Appendix*, Fig. S33), indicating better tissue preservation and more integrated histological continuity compared with other groups. The reduction of glial scars showed a remarkable increase in neurofilament-200 $(NF200)^+$ axons at the lesion site of TPC groups (Fig. 6 *I* and *J* and *SI Appendix*, Fig. S34), which is associated with neurite growth (36). It is worth noting that the regenerated axons in the TPC group also exhibited the most robust remyelination capacity, which aided axon metabolism and signal conduction according to luxol fast blue (LFB) staining (Fig. 6*K* and *SI Appendix*, Fig. S35) (37, 38).

Synaptic signal conduction is the basis of the neural function. To evaluate whether the differentiated neurons could transduce sensory or locomotor signals, immunofluorescence staining was performed for synapsin-1 (Syn-1, mainly serving as a coating protein on synaptic vesicles) and microtubule-associated protein 2 (MAP2, specifically localized in dendrites of mature neurons) (39). Syn-1^+ vesicles were invisible at the lesion sites in the SCI group, while intensive Syn-1^+ puncta were wrapped around the $MAP2^+$

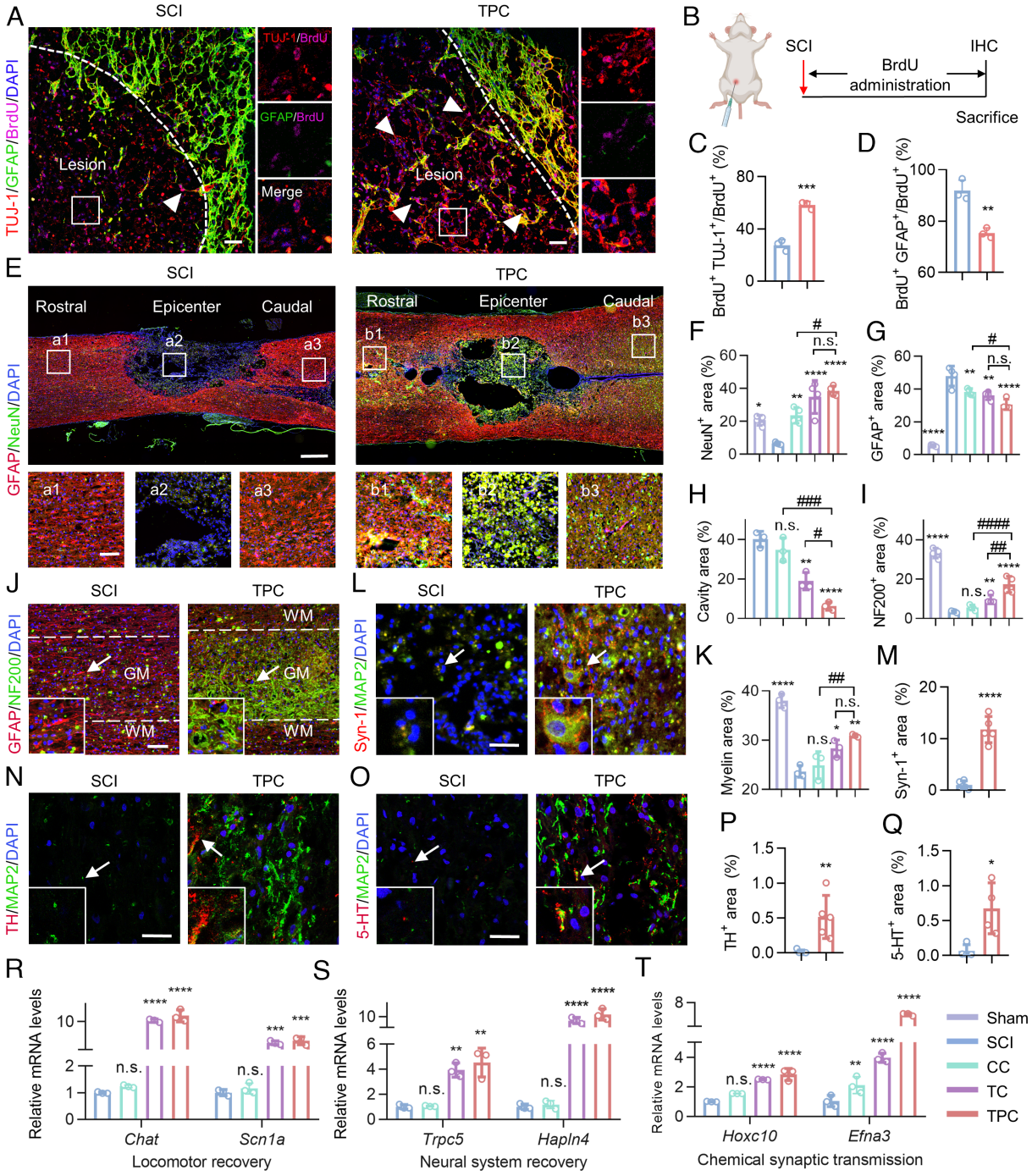

Fig. 6. Promotion of axon regrowth and neural circuit reconstruction in vivo. (*A*) Representative immunostaining images of lesion sites in the SCI and TPC groups at 4 wpi, which were stained with anti-TUJ-1 (red)/anti-GFAP (green)/anti-BrdU (magenta) antibodies and DAPI (blue). Enlarged images of the box regions are shown in the right panel. The white arrows indicate TUJ-1$^+$ BrdU$^+$ cells. White dashed lines indicate the border of lesion areas. (Scale bar: 50 μm.) (*B*) Experimental design for BrdU administration after SCI. (*C*) The proportion of BrdU$^+$ TUJ-1$^+$ cells to BrdU$^+$ cells at the epicenter of lesion areas in SCI and TPC (n = 3) groups. (*D*) The proportion of BrdU$^+$ GFAP$^+$ cells to BrdU$^+$ at the boundary of the lesion areas. (*E*) Representative immunostaining images of lesion areas in the SCI and TPC groups at 8 wpi, which were stained with anti-NeuN antibodies (red), anti-GFAP antibodies (green), and DAPI (blue). White boxes indicate the rostral border (a1 and b1), the epicenter (a2 and b2), and the caudal border (a3 and b3) of injured spinal cords. (Scale bar: 500 μm [*Top*] and 100 μm [*Bottom*].) (*F* and *G*) Quantification of the percentages of NeuN$^+$ (*F*) and GFAP$^+$ (*G*) areas to focal areas (n = 4). (*H* and *I*) Quantification of the percentages of cavity (n = 3) (*H*) and NF200$^+$ (n = 4) (*I*) areas to focal areas. (*J*) Representative immunostaining images of lesion areas in the SCI and TPC groups at 8 dpi, which were stained with anti-NF200 (red)/anti-GFAP (green) antibodies and DAPI (blue). GM, gray matter. WM, white matter. An enlarged view of the box region as indicated with the arrow is shown on the bottom left. The distance of the selected sites from the epicenter of injured spinal cords is 1.5 mm. (*K*) Quantification of the percentages of myelin areas to focal areas (n = 3). (*L*) Representative immunostaining images of lesion areas in the SCI and TPC groups at 8 dpi, which were stained with anti-Syn-1 (red)/anti-MAP2 (green) antibodies and DAPI (blue). (*M*) Quantification of the percentages of Syn-1+ areas to focal areas (n = 5). (*N* and *O*) Representative immunostaining images of lesion areas in the SCI and TPC groups at 8 dpi, which were stained with anti-TH (red)/anti-MAP2 (green) antibodies (*N*), and anti-5-HT (red)/anti-MAP2 (green) antibodies (*O*), respectively. Cell nuclei were stained with DAPI (blue). (*P* and *Q*) Quantification of the percentages of TH$^+$ (n = 5) (*P*) and 5-HT$^+$ (n = 4) (*Q*) areas to focal areas. Scale bar: 100 μm in (*J*), 50 μm in (*L*, *N* and *O*). (*R*–*T*) Relative mRNA levels (qRT-PCR assay) of *Chat* and *Scn1* (*R*), *Hoxc10* and *Efna3* (*S*), and *Trpc5* and *Hapln4* (*T*) of spinal cord tissue in different groups at 8 wpi (n = 3), which were normalized against the sham group. All data represent the mean ± SD. (*F*, *G*, *H*, *I*, *K*, *R*–*T*) One-way ANOVA followed by Tukey's post hoc test; (*C*, *D*, *M*, *P* and *Q*) Student's two-tailed unpaired *t* test. **P* < 0.05, ***P* < 0.01, ****P* < 0.001, and *****P* < 0.0001 compared with SCI group. #*P* < 0.05, ###*P* < 0.001, and ####*P* < 0.0001 compared with TPC group. n.s. = not significant.

cells in the TPC group (Fig. 6 *L* and *M*), suggesting robust synaptogenesis and the spontaneous synaptic activity of neurons. Dopaminergic neurons and serotonergic neurons play important roles in regulating locomotor and sensory functions, where tyrosine hydroxylase (TH) and serotonin (5-HT) are the respective markers (40). The TPC hydrogels significantly promoted the regrowth of locomotor and sensory neurons at the lesion sites (Fig. 6 *N*–*Q*). The average fluorescence intensity of TH^+ and $5\text{-}HT^+$ in the TPC groups were about 30-fold and ninefold higher than those in the SCI group, respectively. Importantly, qRT-PCR confirmed that the mRNA expression of *Chat* and *Scn1a* involved in locomotor recovery, *Hoxc10* and *Efna* 3 involved in chemical synaptic transmission, and *Trpc5* and *Hapln4* involved in neural system recovery were strongly enhanced after TPC treatment (Fig. 6 *R*–*T*). H&E staining of the main organs and blood testing demonstrated that the CC, TC, and TPC hydrogels had negligible toxicity (*SI Appendix*, Fig. S36). Collectively, these results suggest that the TPC hydrogels provide a suitable microenvironment for promoting spontaneous neurogenesis and synaptogenesis.

In conclusion, this work demonstrates that the regulation and detoxification of overloaded iron ions can be achieved using polyphenol-based hydrogels to revitalize neurogenesis after SCI. Iron overloading significantly inhibited neural regeneration and axon outgrowth, increased the risks for neuronal death, and thereby limited locomotor functional recovery after SCI. Polyphenol-based hydrogels were able to restore the iron homeostasis of neurons via the upregulation of the xCT/GPX4 axis, inhibition of GSH depletion, and modulation of iron transportation and metabolism. More importantly, hydrogels integrated with metal-chelating and antioxidant properties fostered the expandable differentiation of newborn NSPCs into neurons and the formation of functional synapses, which contributed to neural network reconstruction and electrophysiological signaling transmission. Polyphenol-based hydrogels as a protective shield for neuronal iron homeostasis represent a promising locoregional therapeutic system to facilitate neurogenesis and function restoration after SCI or iron-accumulating neurological diseases.

Materials and Methods

Preparation and Characterization of Polyphenol-Based Hydrogels. For the preparation of TC hydrogels, CC (M_W 20 to 30 kDa, degree of carboxylation ≈80%, Beijing Solarbio Science & Technology Co., Ltd.) was dissolved in TA (Sigma-Aldrich) solution under vortexing. The mixture was homogenized by stirring, resulting in the formation of hydrogels. For the preparation of the TPC hydrogels, TA solution was mixed with the suspension of PDAR NPs before the dissolution of CC. Specifically, CC (100 mg) was dissolved in 1 mL of TA solution (6 mg/mL) with or without the addition of PDAR NPs (100 μg). Supercritical-dried hydrogels were prepared by dehydrating with a gradient concentration of ethanol and puttered with gold for 180 s at 2 mA before observation by SEM (Zeiss G300).

The Spinal Cord Injury Model. During the surgical procedures, animals were anesthetized with isoflurane. Following laminectomy, the dorsal surface of the T10 spinal cord was exposed. Spinal contusion injury was inflicted using the spinal cord impactor (#68093, RWD, China) with 10 g cylindrical rods (diameter of 2.5 mm, drop height of 50 mm, and hitting depth of 2 mm). Subsequently, different materials were applied onto the dorsal surface of the injured spinal cord, followed by incision close. After the operation, all rats routinely received necessary nursing care, including bladder massage, defecation assistance, and ceftiofur sodium (Amicogen) injection for 7 d. Adult female SD rats (220 to 250 g, SPF Biotechnology) were used in this study, which were divided into five groups: Sham group (removal of the vertebral plate without damage to the spinal cord), SCI group (no treatment except for necessary nursing care), CC group (injection of 20 μL CC scaffold), TC group (injection of 20 μL TC hydrogel), and TPC group (injection of 20 μL TPC hydrogel).

Animals. All animal experiments were approved by the Animal Care and Experiment Committee of Qilu Hospital affiliated to Shandong University (approval No. DWLL-2021-003) and carried out following the local animal care guidelines.

The details of the materials and methods including *Cell Cultures, Intracellular Iron Detection, Immunofluorescence Analysis, MRI Evaluation, Locomotor Function Assessments, RNA Sequencing and Bioinformatics Analysis, Immunohistochemical*, and *Statistical Analysis* are described in *SI Appendix*.

Data, Materials, and Software Availability. All sequencing data generated in this study have been deposited in the Sequence Read Archive (SRA) under accession number of PRJNA1030756 (41). All study data are included in the article and/or supporting information.

ACKNOWLEDGMENTS. The work was funded by the National Natural Science Foundation of China (22072075, 82172740, 82111530202, and 22202119), the Innovation Project of Jinan Science and Technology Bureau (2020GXRC022 and 2021GXRC065), the Natural Science Foundation of Shandong Province (ZR2021LSW008), and the Shandong Foundation for Taishan Scholars (tstp20230656, tsqn202306358). We thank Dr. Zhonghe Zhang at Shandong Provincial Hospital for the MRI characterization. This work was performed in part at the Analytical Centre for Structural Constituent and Physical Property, and the Translational Medicine Core Facility of Advanced Medical Research Institute at Shandong University.

Author affiliations: [a]Key Laboratory of Colloid and Interface Chemistry of the Ministry of Education, School of Chemistry and Chemical Engineering, Shandong University, Jinan, Shandong 250100, China; [b]Department of Neurosurgery, Qilu Hospital of Shandong University, Institute of Brain and Brain-Inspired Science, Cheeloo College of Medicine, Shandong University, Jinan, Shandong 250012, China; [c]Shandong Key Laboratory of Brain Function Remodeling, Jinan, Shandong 250117, China; and [d]Department of Endocrinology, Qilu Hospital of Shandong University, Cheeloo College of Medicine, Shandong University, Jinan, Shandong 250012, China

1. F. B. Wagner *et al.*, Targeted neurotechnology restores walking in humans with spinal cord injury. *Nature* **563**, 65–71 (2018).
2. J. Koffler *et al.*, Biomimetic 3D-printed scaffolds for spinal cord injury repair. *Nat. Med.* **25**, 263–269 (2019).
3. Y. Bi *et al.*, Neutrophil decoys with anti-inflammatory and anti-oxidative properties reduce secondary spinal cord injury and improve neurological functional recovery. *Adv. Funct. Mater.* **31**, 2102912 (2021).
4. E. J. Bradbury, E. R. Burnside, Moving beyond the glial scar for spinal cord repair. *Nat. Commun.* **10**, 3879 (2019).
5. S. Thuret, L. D. Moon, F. H. Gage, Therapeutic interventions after spinal cord injury. *Nat. Rev. Neurosci.* **7**, 628–643 (2006).
6. L. Shen *et al.*, Ferroptosis in acute central nervous system injuries: The future direction? *Front. Cell Dev. Biol.* **8**, 594 (2020).
7. Y. Chen *et al.*, The latest view on the mechanism of ferroptosis and its research progress in spinal cord injury. *Oxid. Med. Cell. Longev.* **2020**, 6375938 (2020).
8. B. R. Stockwell, Ferroptosis turns 10: Emerging mechanisms, physiological functions, and therapeutic applications. *Cell* **185**, 2401–2421 (2022).
9. J. Li *et al.*, Ferroptosis: Past, present and future. *Cell Death Dis.* **11**, 88 (2020).
10. S. J. Dixon *et al.*, Ferroptosis: An iron-dependent form of nonapoptotic cell death. *Cell* **149**, 1060–1072 (2012).
11. L. J. Routhe, T. Moos, Handling iron in restorative neuroscience. *Neural Regen. Res.* **10**, 1558–1559 (2015).
12. Y. Ju, H. Liao, J. J. Richardson, J. Guo, F. Caruso, Nanostructured particles assembled from natural building blocks for advanced therapies. *Chem. Soc. Rev.* **51**, 4287–4336 (2022).
13. H. Geng *et al.*, Metal ion-directed functional metal–phenolic materials. *Chem. Rev.* **122**, 11432–11473 (2022).
14. H. Zeng, D. S. Hwang, J. N. Israelachvili, J. H. Waite, Strong reversible Fe^{3+}-mediated bridging between dopa-containing protein films in water. *Proc. Natl. Acad. Sci. U.S.A.* **107**, 12850–12853 (2010).
15. L. Q. Xu, K.-G. Neoh, E.-T. Kang, Natural polyphenols as versatile platforms for material engineering and surface functionalization. *Prog. Polym. Sci.* **87**, 165–196 (2018).
16. H. Ejima *et al.*, One-step assembly of coordination complexes for versatile film and particle engineering. *Science* **341**, 154–157 (2013).
17. J. Guo *et al.*, Modular assembly of superstructures from polyphenol-functionalized building blocks. *Nat. Nanotechnol.* **11**, 1105–1111 (2016).
18. R. G. Andrade Jr. *et al.*, Tannic acid inhibits in vitro iron-dependent free radical formation. *Biochimie* **88**, 1287–1296 (2006).
19. N. R. Perron, J. N. Hodges, M. Jenkins, J. L. Brumaghim, Predicting how polyphenol antioxidants prevent DNA damage by binding to iron. *Inorg. Chem.* **47**, 6153–6161 (2008).

20. C. Pucci *et al.*, Tannic acid–iron complex-based nanoparticles as a novel tool against oxidative stress. *ACS Appl. Mater. Interfaces* **14**, 15927–15941 (2022).
21. H. Lee *et al.*, Iron gall ink revisited: In situ oxidation of Fe(II)–tannin complex for fluidic-interface engineering. *Adv. Mater.* **30**, 1805091 (2018).
22. S.-Q. Feng *et al.*, Liproxstatin-1 is an effective inhibitor of oligodendrocyte ferroptosis induced by inhibition of glutathione peroxidase 4. *Neural Regen. Res.* **16**, 561–566 (2021).
23. W. S. Yang, B. R. Stockwell, Synthetic lethal screening identifies compounds activating iron-dependent, nonapoptotic cell death in oncogenic-RAS-harboring cancer cells. *Chem. Biol.* **15**, 234–245 (2008).
24. F. De Virgiliis *et al.*, Enriched conditioning expands the regenerative ability of sensory neurons after spinal cord injury via neuronal intrinsic redox signaling. *Nat. Commun.* **11**, 6425 (2020).
25. L. Zhou *et al.*, Soft conducting polymer hydrogels cross-linked and doped by tannic acid for spinal cord injury repair. *ACS Nano* **12**, 10957–10967 (2018).
26. X. Yao *et al.*, Deferoxamine promotes recovery of traumatic spinal cord injury by inhibiting ferroptosis. *Neural. Regen. Res.* **14**, 532–541 (2019).
27. K. Jin, X. Wang, L. Xie, X. O. Mao, D. A. Greenberg, Transgenic ablation of doublecortin-expressing cells suppresses adult neurogenesis and worsens stroke outcome in mice. *Proc. Natl. Acad. Sci. U.S.A.* **107**, 7993–7998 (2010).
28. S. F. Sorrells *et al.*, Human hippocampal neurogenesis drops sharply in children to undetectable levels in adults. *Nature* **555**, 377–381 (2018).
29. R. D. Horniblow, D. Henesy, T. H. Iqbal, C. Tselepis, Modulation of iron transport, metabolism and reactive oxygen status by quercetin-iron complexes in vitro. *Mol. Nutr. Food Res.* **61**, 1600692 (2017).
30. E. M. Terzi, V. O. Sviderskiy, S. W. Alvarez, G. C. Whiten, R. Possemato, Iron-sulfur cluster deficiency can be sensed by IRP2 and regulates iron homeostasis and sensitivity to ferroptosis independent of IRP1 and FBXL5. *Sci. Adv.* **7**, eabg4302 (2021).
31. E. Gammella, P. Buratti, G. Cairo, S. Recalcati, The transferrin receptor: The cellular iron gate. *Metallomics* **9**, 1367–1375 (2017).
32. Y. Sun *et al.*, The emerging role of ferroptosis in inflammation. *Biomed. Pharmacother.* **127**, 110108 (2020).
33. Q. Mu *et al.*, The role of iron homeostasis in remodeling immune function and regulating inflammatory disease. *Sci. Bull.* **66**, 1806–1816 (2021).
34. J. Park *et al.*, Intravascular innate immune cells reprogrammed via intravenous nanoparticles to promote functional recovery after spinal cord injury. *Proc. Natl. Acad. Sci. U.S.A.* **116**, 14947–14954 (2019).
35. K. Shen *et al.*, Anti-inflammatory nanotherapeutics by targeting matrix metalloproteinases for immunotherapy of spinal cord injury. *Small* **17**, 2102102 (2021).
36. Z. Li *et al.*, Nervous tract-bioinspired multi-nanoyarn model system regulating neural differentiation and its transcriptional architecture at single-cell resolution. *Biomaterials* **298**, 122146 (2023).
37. Y. Lee *et al.*, Oligodendroglia metabolically support axons and contribute to neurodegeneration. *Nature* **487**, 443–448 (2012).
38. Y. Shi *et al.*, Effective repair of traumatically injured spinal cord by nanoscale block copolymer micelles. *Nat. Nanotechnol.* **5**, 80–87 (2010).
39. A. Marchini *et al.*, Multifunctionalized hydrogels foster hNSC maturation in 3D cultures and neural regeneration in spinal cord injuries. *Proc. Natl. Acad. Sci. U.S.A.* **116**, 7483–7492 (2019).
40. Z. Álvarez *et al.*, Bioactive scaffolds with enhanced supramolecular motion promote recovery from spinal cord injury. *Science* **374**, 848–856 (2021).
41. Z. Li, Restoring neuronal iron homeostasis revitalizes neurogenesis after spinal cord injury. NCBI Sequence Read Archive (SRA). http://www.ncbi.nlm.nih.gov/bioproject/1030756. Deposited 21 October 2023.